Journal of Renewable Energy and Sustainable Development (RESD)
Volume 12, Issue 1, June 2026 - ISSN 2356-8569
http://dx.doi.org/10.21622/RESD.2026.12.1.1765

Received: 03 November 2025 Accepted: 25 January 2026 Published: 6 April 2026

Parametric Study and Performance Analysis of Flanged Diverging Diffusers for Small Wind Turbines

Mangesh R. Mahajan [1*], Sanjay D. Nikhade [2], and Sandip A. Kale [3]

[1*,2] Sandip University, School of Engineering & Technology, Mechanical Engineering Department, Mahiravani, Tryambak road, Nashik, India

[1*] Dr. Vishwanath Karad MIT World Peace University, Kothrud, Pune, India

[3] Technology Research and Innovation Centre, Dhayari, Pune, India

mangesh.mahajan@mitwpu.edu.in, sanjaynikhade@rediffmail.com, sandipakale2050@gmail.com

Abstract

Flanged diverging diffusers are advantageous because of higher durability, lower mass and cost, better environmentally friendly design, compared to various diffuser models used to increase the wind velocity at wind turbine rotor planes. Diffuser length, expansion angle, and flange height affect the diffuser performance in terms of velocity enhancement and mass. This study has systematically used Design of Experiments (DOE) for these three parameters at five levels. The computational Fluid Dynamics (CFD) simulations are performed for a total of twenty-five diffuser models obtained using DOE. The results of one selected CFD model are validated with wind tunnel experimentation, showing acceptable agreement. CFD results are further examined using multivariate regression analysis, Pareto Charts, main effect plots, 2D interaction contours, and 3D surface response plots. The obtained regression equation delivers the predicted accuracy. Among the parameters, the expansion angle is observed as an important factor that influences the velocity output, followed by the diffuser length and flange height. Further, the optimum dimensions of the diffuser are found using desirability function analysis, which suggests the intermediate value of diffuser length, lower values of expansion angle, and flange height provide compromised velocity performance with significantly reduced mass and cost.

Index-words: *CFD, Diffuser Augmented Wind Turbine, Small Wind Turbine, Optimization.*

I. Introduction

Use of major electricity-consuming devices for domestic applications is continuously increasing. To meet the demands of a modern lifestyle, the power requirements of manufacturing and service industries are also rising significantly [1, 2]. Additionally, in many developing countries, the acceptance of electric vehicles for transportation is growing rapidly. To meet these increasing energy requirements and due to increasing awareness about global warming, individuals, researchers, scientists, and governments have accepted the significance of renewable energies [3-9]. Amongst various renewable energies, solar and wind energy have significant potential to fulfill the growing demand for electricity with sustainable development [10-12].

The electric power produced through any wind turbine rotor is based on the conversion of wind's kinetic energy into rotational energy. The wind turbine power output could be enhanced by increasing the wind velocity at the rotor plane. This can be achieved by surrounding the rotor using an accelerator, commonly termed a diffuser. Small wind turbines combined with diffusers have significant potential to generate electricity even at low wind speeds [13-18]. Many researchers have reported multi-fold increases in power output using diffusers as compared to bare wind turbines using different theories, computational simulations, and experiments. Various diffuser designs are studied by these researchers and found varying performance in terms of accelerating the wind velocity with respect to the free stream wind velocity. The current research trends in this field include studies on the modification and development of various shapes and parametric evaluation using computational and experimental techniques.

* Corresponding author

Volume 12, Issue 1, June 2026 - ISSN 2356-8569
http://dx.doi.org/10.21622/RESD.2026.12.1.1765

Basic diffuser types include conical diverging diffusers, converging-diverging diffusers, and airfoil-shaped diffusers. These diffusers are studied with and without flanges. Researchers are also investigating modifications to these basic designs, such as changing geometries, adding new components, and multi-staging of basic shapes in order to improve the approaching wind velocity at the wind turbine rotor [3, 14, 19-22]. Although various diffuser shapes have been proposed by researchers to improve small wind turbines' power, the basic diverging diffuser with a flange has significant capability to accelerate wind velocity [23-26]. This research paper focuses specifically on the diverging diffuser with flange due to its design simplicity, manufacturing ease, and established effectiveness in previous research studies.

The diverging diffuser has four dimensional parameters: 1) inlet diameter *(D)*, 2) length of diffuser *(L)*, 3) semi-expansion angle *(α)*, and 4) height of flange *(h)* as presented by Fig. 1. The outlet diameter (D_o) is a dependent parameter and changes with respect to semi-expansion angle and diffuser length. The summary of previous research works about diverging diffusers with and without a flange is presented below. In this summary, for easy evaluation, the description is based on dimensionless parameters. These dimensionless parameters are expressed in terms of the inlet diameter. The first dimensionless parameter is used to define diffuser length and expressed as length to diameter ratio *(L/D)*, and the Second dimensionless parameter is used to define flange height and expressed as flange height to diameter ratio *(h/D)*.

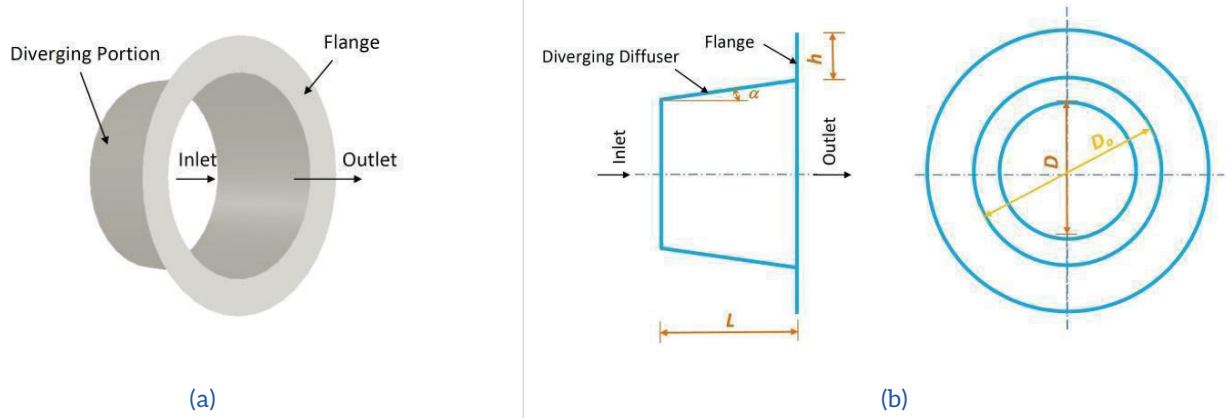

Figure 1: Terminology of a diverging diffuser with flange.

Badawy and Ali (2000) theoretically studied the velocity enhancement for diffusers without flanges at seven levels of length and angle. They considered lengths ranging from 1 to 7 times the entry diameter and semi-expansion angles from 0 ° to 15 °, respectively, and claimed an augmentation ratio of up to 7. Though the augmentation is impressive, its use can be limited by considerably higher diffuser lengths [27]. Abe and Ohya (2004) presented the computational study of diffusers with and without flanges. They considered four different *h/D* ratios as 0, 0.125, 0.25, and 0.5, and also two semi-expansion angles as 4 ° and 15 °. They found that the flanged diffuser performance is significantly based on the angle and loading coefficient [28].

An experimental study by Matsushima *et al.* (2006) claimed a 1.7 times velocity enhancement for a diverging diffuser with *an L/D* ratio of 2 and a semi-expansion angle of 4 °. They have also reported the CFD results for varying *L/D* from 0.4 to 3 in seven variable 7 levels, seven levels of semi-expansion angles from 0 to 12 ° in steps of 2 °, and six levels of flange height in terms of *h/D*, ranging from 0 to 0.5 *h/D*. This CFD study was conducted by fixing some parameters, focusing on specific configurations rather than using a systematic design of experiments [29].

Ohya *et al.* (2008) experimentally studied the fixed-length (1.25 D) diffusers with seven *h/D* ratios from 0 to 0.625 in steps of 0.125, semi-expansion angle of 4°, and claimed considerable power output compared to bare wind turbines [30]. The diverging diffuser experimental study by Kosasih and Tondelli (2012) at *L/D* and *h/D* ratios ranging from 0.63 to 1.5 and 0 to 0.2, respectively, at a fixed expansion angle of 12 ° compared with the converging-diverging diffuser claimed only 1.7 % less performance [31].

Barbosa *et al.* (2013) studied a diffuser with a 40 semi-expansion angle and an *L/D* ratio of 0.75 and

Volume 12, Issue 1, June 2026 - ISSN 2356-8569
http://dx.doi.org/10.21622/RESD.2026.12.1.1765

claimed good agreement between experimental and analytical results with a velocity enhancement ratio of about 1.22 [32]. Jafari and Kosasih (2014) used short-length diffusers with four levels L/D ranging from 0.1 to 0.4 and 14 levels h/D ranging from 0.025 to 0.35 in steps of 0.025. They observed that the h/D ratio can be limited to 0.05 to 0.15 for selected lengths. [33].

In a research by Roshan *et al.* (2015), 1.19 times velocity enhancement is observed for a flangeless diffuser of L/D = 0.54 and semi-expansion angle of 9 ° [34]. Lipian *et al.* (2015) have carried out a study to identify the potential of diverging diffusers for small wind turbines using computational and experimental methods. They analyzed diffusers for a fixed L/D ratio of one, three h/D ratios (0.1, 0.3, and 0.5) at sixteen different semi-expansion angles from 0 ° to 15 °. They obtained mixed velocity improvements at various positions for said combinations [35]. Olasek *et al.* (2016) performed an experimental study for three different dimensions with the same dimensional proportion as L/D = 1, h/D = 0.1, and a semi-expansion angle of 2.12 °. They observed 70-75 % power enhancement [36].

Masukume *et al.* (2016) conducted research on various diverging diffusers without a flange. They considered six levels of two variables. L/D ratios experimented with ranged from 0.5 to 3 with fixed steps, and semi-expansion angles used were 3.5 °, 4.5 °, 5.5 °, 7.5 °, 11 °, and 14 °. They observed better performance at an L/D ratio of 2 [37]. The comprehensive study on the effect of surface roughness on wind turbine blade performance was carried out by Zidane et al. (2016). The authors showed that roughness can result in the boundary layer thickening along with a change in the location of (early) transition, which can substantially reduce power output. DAWTs shall be smooth in order to have a better flow acceleration [38]. El-Zahaby *et al.* (2017) have conducted computational analysis for diverging diffusers with *an* L/D ratio of 1.5 and a semi-expansion angle of 3.18 °, *and a* h/D ratio of 1.25. Further, they studied velocity enhancement at various flange inclinations and found marginal changes for positive angles [39]. Zidane et al. (2017) carried out a CFD investigation on transitional separation bubble characteristics using the NACA 63415 airfoil at lower Reynolds numbers. The studies focused on the effect of development, growth, and reattachment of separation bubbles on the lift and drag experienced during laminar–turbulent transition and separation of flow. Bubble separation can affect the local increase of Reynolds number at the rotor [40].

Zidane et al. (2017) studied the effect of contaminated or dusty air flow on the performance of NACA 63415 airfoil blades. The findings were interesting and showed that the dusty flow can alter pressure distribution, boundary layer, and thus overall performance. Changes in lift and drag coefficients were also reported. [41] Masukume *et al.* (2018) have conducted an experimental study for a diverging diffuser without a flange at L/D = 0.5 and semi-expansion angle of 14.5 ° and reported a power enhancement of 2.5 times [42]. Takey *et al.* (2020) performed a computational investigation on a short diffuser of L/D ratio 0.23, h/D = 0.1, and semi-expansion angle of 10 ° and found better performance than that of without a flange and only a flange [43].

Zidane et al (2020) use machine learning techniques to investigate the effect of sandstorms on the performance of wind turbine blades. The drag force increases and the lift force reduces due to the presence of sand, which alters aerodynamic forces [44]. İlhan *et al.* (2021) studied different dimensional combinations of diverging diffusers. Their first group consists of four diffusers with a fixed L/D ratio of 1.4 and a semi-expansion angle of 9^0, and four different h/D ratios from 0 to 0.4 with constant intervals. The second group includes six diffusers with a fixed L/D ratio of 1.35 and semi-expansion angles of 3 °, 4 °, 5 °, 6 °, 9 °, and 12 (variable intervals) with a fixed h/D ratio of 0.2. The third group comprises five diffusers with fixed h/D as 0.2 and semi-expansion angle 6 ° with variable L/D values from 1.3 to 1.5, having a constant interval. The computational analysis found velocity enhancements of 1.511, 1.567, and 1.584 times the free wind velocity in these three groups [45]. Mohanan *et al.* (2021) conducted computational research on diffusers without flanges at semi-expansion angles of 2 °, 3 °, and 5 ° with an exit diameter equal to the diffuser length. They found better performance at low angles [46]. Rahmatian *et al.* (2022) reproduced results for a conical diverging diffuser of L/D = 1.5, α = 4 ° and h/D = 0.5, and compared with the modified diffuser [47].

Zidane *et al.* (2023) used upstream deflectors, which improved the performance of the H-Darrieus wind turbine. The study also optimizes the geometrical configuration of deflectors to have a better performance [48]. Abdallah et al. (2024)

Volume 12, Issue 1, June 2026 - ISSN 2356-8569
http://dx.doi.org/10.21622/RESD.2026.12.1.1765

and Abdallah et al. (2025) showed performance enhancement of the H-Darrieus type of vertical axis wind turbine (VAWT) by using innovative J-shaped blade geometries. CFD analysis was carried out, which revealed better starting torque, delayed flow separation, and enhanced aerodynamic efficiency. The J-blade approach is compatible with Diffuser Augmented Wind Turbines, both of which reveal geometry-induced flow guidance that can be used to improve energy extraction, especially in low-speed areas [49, 50].

Through the literature reading, it is noticed that the diverging diffuser performance depends not only on one or two parameters but on all three-dimensional parameters *(L/D, h/D,* and *α)*. Most of the reported research works either performed research using one or two variables. Few researchers studied the effect of all three parameters, but with uneven intervals as well as different parametric evaluations. Also, the consideration of mass during diffuser design is very rarely observed in the literature.

This work is carried out to study the influence of input variables *(L/D, h/D,* and *α)* on the diffuser performance using a systematic Design of Experiments (DOE) approach. For each of these three parameters, five levels *(L/D* = 0.5 to 1.5, *h/D* = 0.1 to 0.5, and *α* = 3 ° to 15 °) are selected, and computational Fluid Dynamics (CFD) of all twenty-five diverging diffusers with flange is carried out using ANSYS FLUENT 2022 R1. In addition to velocity performance evaluation, it is important to study diffuser bulkiness, which is also one of the barriers to placing them in actual applications. Hence, the effect of input variables on the mass of the diffuser is also included in this study.

Hence, this study used systematic Taguchi-based optimization, including mass as a second objective. In this research work, all three parameters are symmetrically varied within considerable ranges. Results are also evaluated using appropriate statistical techniques on the basis of velocity enhancement as well as the bulkiness of the diffuser in the form of mass. The current research results are also validated with experimental results.

II. Materials and Methods

As per the defined scope of the present research, it was decided to study the influence of all three input independent variables *(L/D, h/D,* and *α)* on the performance of the diffuser. This performance can be measured in terms of velocity augmentation. The computational experiments are designed using the Taguchi Orthogonal array method. Computational fluid dynamics (CFD) simulations are performed using ANSYS FLUENT 2022 R1. The following subsections describe the procedure for the design of experiments and the CFD procedure used for this research.

A. Design of experiments

In the current study of the diverging diffuser, there are three independent variables: *L/D, h/D,* and *α,* which change the output performance (V_x) and mass of the diffuser. The randomly developed experiments may not give insight into the effect of input variables on the output variables. In such cases, appropriate statistical techniques can be useful to decide various combinations of diffuser dimensions in order to get better velocity output. Well, the acceptable Design of Experiments (DOE) used for product or process design is also used by many researchers for CFD studies [45-48]. In the current research, five levels of each parameter are proposed, which requires a total of 125 (5^3 = 125) experiments.

Table 1: Parameter levels finalized for the Taguchi arrays

Parameters	Level 1	Level 2	Level 3	Level 4	Level 5
L/D	0.5	0.75	1	1.25	1.5
α (°)	3	6	9	12	15
h/D	0.1	0.2	0.3	0.4	0.5

Table 2: L_{25} (P = 3, L = 5) Orthogonal array for the study of velocity enhancement

Model	*L/D*	*α*	*h/D*
C01	0.5	3	0.1
C02	0.5	6	0.2
C03	0.5	9	0.3
C04	0.5	12	0.4
C05	0.5	15	0.5
C06	0.75	3	0.2
C07	0.75	6	0.3
C08	0.75	9	0.4
C09	0.75	12	0.5
C10	0.75	15	0.1
C11	1	3	0.3
C12	1	6	0.4

Volume 12, Issue 1, June 2026 - ISSN 2356-8569
http://dx.doi.org/10.21622/RESD.2026.12.1.1765

C13	1	9	0.5
C14	1	12	0.1
C15	1	15	0.2
C16	1.25	3	0.4
C17	1.25	6	0.5
C18	1.25	9	0.1
C19	1.25	12	0.2
C20	1.25	15	0.3
C21	1.5	3	0.5
C22	1.5	6	0.1
C23	1.5	9	0.2
C24	1.5	12	0.3
C25	1.5	15	0.4

Using Taguchi orthogonal arrays, it is possible to design only 25 computational experiments, $L_{25}(5^3)$ (orthogonal matrix array), to analyze the velocity performance appropriately for three variables with five levels. In the $L_{25}(5^3)$ array, 'L' represents the orthogonal array with a total of 25 samples for study, including 3 variables and 5 levels [51].

As shown in Table 1, length-to-diameter ratios (L/D) are taken from 0.5 to 1.5 with a fixed interval of 0.25. Second-dimensional variable - semi-expansion angles (α) range from 3 ° to 15 ° in steps of 3 °. The third input variable (h/D) starts at 0.1 and ends at 0.5 with an increment of 0.1. Inlet diameter for all models is kept fixed. The models used for these computational analyses are named as C01 to C25, respectively, and shown in Table 2. Each of the independent variables is tested five times. The scope of this study is limited to short and medium diffuser lengths. Maximum L/D is limited to 1.5 as the feasibility of long diffusers reduces because of higher mass, bulkiness, handling, and installation difficulties.

To analyze the results effectively, the mass of the diffuser models is taken dimensionless and normalized appropriately. The extreme mass of a diffuser with maximum dimension is considered as a unit, and other diffuser masses are normalized accordingly. So all normalized masses (m_n) are scaled from 0.22 to 1. Here, the parameter - normalized mass is used only to represent compactness and relative material usage among different diffuser configurations. This is taken on the basis of geometry with a uniform wall thickness of 3 mm. For all models, Glass Reinforced Plastic with a density of 1600 kg/m^3 is considered. The detailed structural requirements, material strength, or manufacturing constraints are not included in the scope of this research. Here, the primary objective is to evaluate the aerodynamic performance of different diffuser geometries. Hence, structural analysis, thickness optimization, and cost analysis are purposely excluded from the current scope.

B. *Modeling for computational analysis*

For all diffuser models, the inlet diameter is fixed at 210 mm, and other dimensions are proportioned accordingly. In order to get correct flow details, the inside diffuser's appropriate domain size is important. The inlet of the diffuser is positioned at a distance of 3D from the domain inlet. Performances of diffusers for three different domain lengths, 6D, 12D, and 18D, are studied, and no significant difference is found for domain lengths 12D and 18D. Hence, the domain of upstream length 3D and downstream length 12D is taken for this study, as shown in Fig. 2. The width of the domain is taken as 8D.

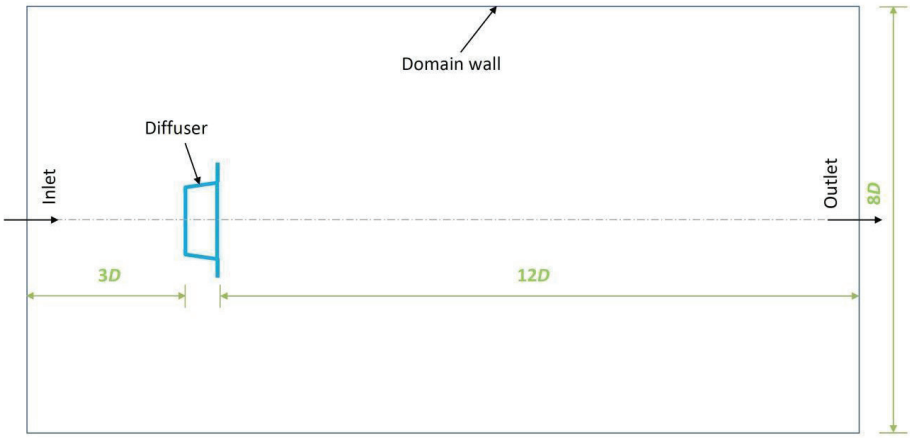

Figure 2: Domain dimensions used for CFD analysis.

Volume 12, Issue 1, June 2026 - ISSN 2356-8569
http://dx.doi.org/10.21622/RESD.2026.12.1.1765

From this, it is observed that there is no significant difference in the third and fourth cell counts. Hence, the mesh size with 62818 cell count is finalized. For other models, the same size mesh quality was defined. Full diffuser mesh view with domain and magnified mesh view of partial diffuser portion indicating the fine mesh used inside and downside of the diffuser are shown in Fig. 3 (a) and (b), respectively.

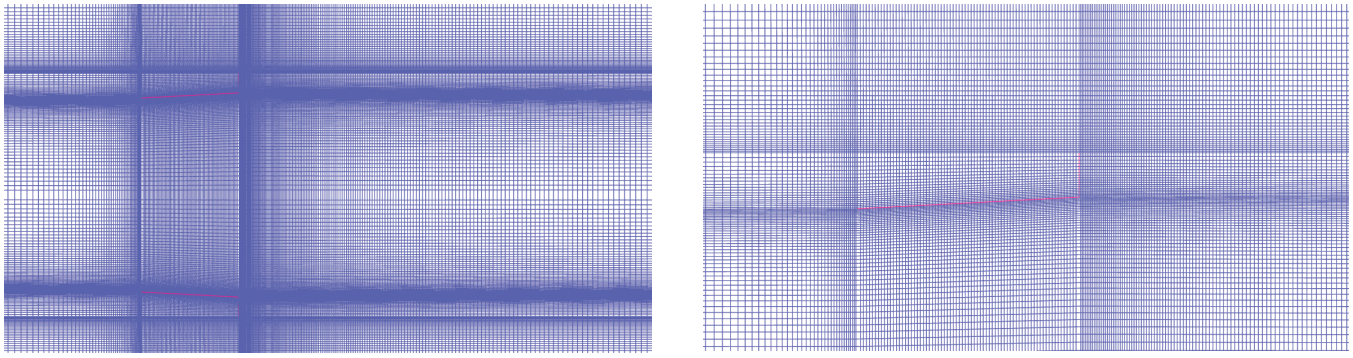

(a) Full diffuser mesh view with domain

(b) Magnified mesh view of diffuser portion

Figure 3: Sample mesh view of a diffuser model C01.

During CFD analysis, it is important to select a suitable model for solving the problem. Many researchers have preferred k-ω Shear Stress Transport (SST) for analyzing flow through diffusers. In this model, turbulent kinetic energy and turbulent specific dissipation rate are represented by k and ω, respectively, and given by two transport equations, Eq. 1 and Eq. 2 [24].

$$\frac{\partial}{\partial t}(\rho K)+\frac{\partial}{\partial x_i}(\rho K u_i)=\frac{\partial}{\partial x_j}\left(\Gamma_K \frac{\partial k}{\partial x_j}\right)+{}_{\tilde{G}}K-Y_k+S_k \quad (1)$$

$$\frac{\partial}{\partial t}(\rho \omega)+\frac{\partial}{\partial x_i}(\rho \omega u_i)=\frac{\partial}{\partial x_j}\left(\Gamma_\omega \frac{\partial \omega}{\partial x_j}\right)+G_\omega-Y_\omega+D_\omega+S_k \quad (2)$$

Where,

${}_{\tilde{G}}K$	=	The result of mean velocity gradients creating turbulent kinetic energy
$G\omega$	=	generation of ω
ΓK	=	effective diffusivity of k
$\Gamma\omega$	=	effective diffusivity of ω
Yk	=	dissipation of k due to turbulence
$Y\omega$	=	dissipation of ω due to turbulence
$D\omega$	=	cross-diffusion term
Sk and $S\omega$	=	user-defined source terms

SST appropriately combines the k- ε and k-ω during the change of distance from the wall. This model is well accepted for diffuser studies because of its accuracy and robustness. Further, as expected in the case of diffuser simulations, this model has a good ability to solve flow separation problems, transition from near and far from wall regions, shear flows, and comparatively less computational time [10, 16, 47, 51-53].

For the computational domain, an unstructured mesh was used, and a high quality (orthogonality) of 0.99 is observed. The simulation was carried out in a two-dimensional axisymmetric domain to reduce computational time without affecting the results. A no-shear condition was applied on the diffuser wall, and specified shear conditions were applied on the domain walls. Incompressible, turbulent flow is considered here. Constant air density is taken as 1.225 kg/m^3. The inlet velocity for all case studies is taken as 6 m/s. Turbulence intensity at the inlet and outlet was set to 2%. The output of the computational domain is set to atmospheric pressure. The residual convergence criterion was fixed at 0.0001. Maximum iterations allowed were set to 1000. The mesh aspect ratio was maintained within acceptable limits, with a maximum value of 4 in the diffuser region and 55 in the fluid domain. The total number of cells varies from 66444 for C01 to 211224 for C25.

The near-wall mesh quality was evaluated using the non-dimensional wall distance (Y^+) at different wall locations. Area-weighted average Y^+ values were obtained for the flange, diffuser wall, and domain wall regions. The Y^+ values ranged from

Volume 12, Issue 1, June 2026 - ISSN 2356-8569
http://dx.doi.org/10.21622/RESD.2026.12.1.1765

2.53 to 5.52 near the diffuser walls. Very low values were observed near the domain wall. The overall net Y^+ value was observed as 0.14. For the SST k–ω turbulence model, Y^+ values close to one are preferred to get accurate flow near the wall. The near-wall Y^+ values in the diffuser region were observed within the acceptable range and hence with sufficient refinement near the walls. Here, the diffuser wall region is critical for obtaining velocity gradients and flow behavior. Hence, the Y^+ distribution is considered satisfactory.

C. Wind tunnel testing

To validate the CFD results, it is decided to test a diffuser using a wind tunnel. For wind tunnel experimentation, diffuser model C01 is selected. The wind tunnel testing is carried out at the Aerodynamics Lab, Defence Institute of Advanced Technology, Girinagar, Khadakwasla, Pune, India. The experimental setup, along with the tested diffuser, is shown in Fig. 4. A Pitot tube (Make Dwyer) and a micro-manometer (Make ACIN Instrumentation) were used during this experimentation. The initial velocity of air in the tunnel was set to 6 m/s (ΔP = 22 Pa). The diffuser was placed inside the tunnel. Using pitot tube readings, the velocity of air is measured at nine different points along a considered plane inside the diffuser. This plane is considered at a plane at x = 0.2L from the diffuser inlet. These nine points were selected at equidistant intervals from the axis and moving towards the diffuser wall. The pitot tube is inserted from the outlet side of the diffuser in order to take a reading from the undisturbed flow.

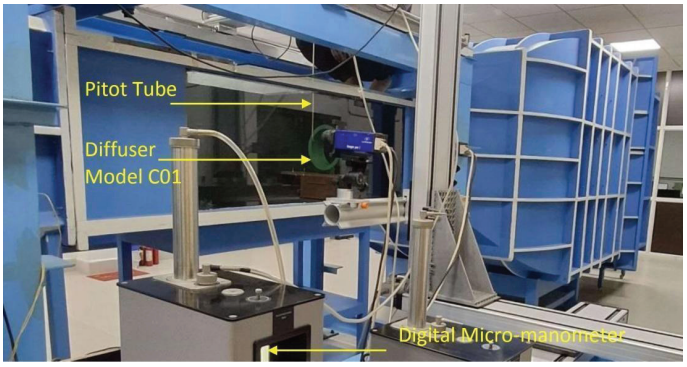

Figure 4: Wind tunnel experimental setup.

The 25 diffuser geometries considered in the study differ in terms of diffuser angle, diffuser length, and flange height. The overall geometry remains fundamentally the same. No additional features, such as steps or slots, are introduced that would result in a drastic alteration of the flow physics. Experimental testing of a single diffuser configuration is sufficient, as it can help in validating the CFD results. This approach is consistent with prior studies reported in the literature, where experimental investigations are commonly limited to a single diffuser out of those under study.

D. Data analysis

As discussed earlier, CFD results are important to know the diffuser models' performance. Identifying the limitations of visual observations of velocity contours obtained through CFD, it is decided to use suitable statistical techniques for a detailed evaluation. It is decided to get the multivariate regression equation to identify the effect of linear terms, quadratic terms, and interaction terms to get an effect in detail. Also, it is decided to use Pareto charts, whose visual observation can deliver some important directions. Further to study the interaction between two input variables, it is decided to plot the 2D contours and 3D surface response plots.

E. Diffuser dimensions optimization and validation

Optimum dimensions of the diffuser $(L/D,\ h/D,\ \alpha)$ to get the higher velocity ratio and lower diffuser mass are obtained using the desirability function analysis (DFA). The predicted performance of this optimized diffuser, as suggested by DFA, is validated with the CFD results. The objective of the present research is limited to the design and optimization of the diffuser geometry. The wind turbine rotor, its dimensions, and performance are assumed fixed throughout the study. Therefore, the optimization is performed on the basis of velocity enhancement along with diffuser mass, rather than overall turbine performance parameters. This allows a focused research on the effectiveness of diffuser models independent of rotor characteristics. Modeling of the turbine rotor, determination of the power coefficient, and detailed power output analysis are planned as part of future studies.

III. Results

A. Velocity contours from CFD

During the computational fluid analysis for all diffuser models, the inlet velocity (V_{in}) is taken as 6 m/s to maintain uniformity of simulation results.

Volume 12, Issue 1, June 2026 - ISSN 2356-8569
http://dx.doi.org/10.21622/RESD.2026.12.1.1765

The velocity contours obtained from CFD for 25 computational experiments are shown in Fig. 5. These velocity contours show the regions with different velocity magnitudes in m/s. The velocity contours in this figure are arranged in such a structured way for easier comparison and analysis. Each row is assigned for diffuser length to diameter ratio *(L/D)*, and each column is assigned for semi-expansion angle *(α)*. The third variable *(h/D)* varies across each plot. As can be seen from Table 3, *L/D* ratios vary from 0.5 to 1.5, whereas *h/D* ratio varies from 0.1 to 0.5

Diffuser models obtained through the DOE orthogonal array $L_{25}(5^3)$ with three parameters and five levels, together with their response, are shown in Table 3. In this table, velocities are presented in dimensionless form (V_x/V_{in}) and represented by the velocity ratio (V_R). V_x is taken as the maximum velocity obtained inside the diffuser. This table also includes the normalized masses for these diffuser models. The mass of all diffusers is calculated using a common throat diameter for all the diffusers, and automatically, all other dimensions can be obtained.

B. Experimental validation of CFD results

The pressure values recorded from the experimental setup are converted into velocity values using Eq. 3

$$V = \sqrt{\frac{2(P_0 - P_s)}{\rho}} \tag{3}$$

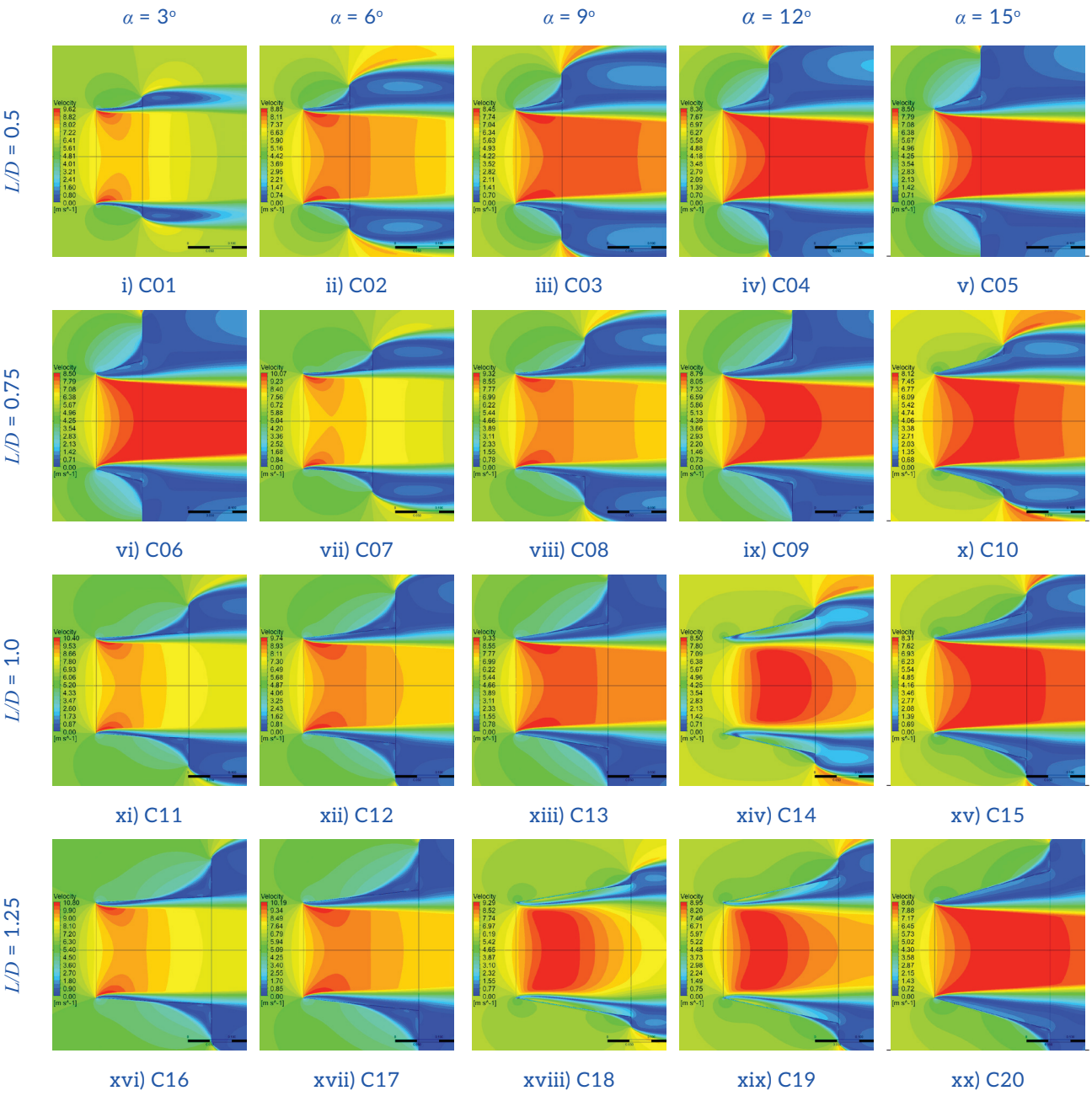

Volume 12, Issue 1, June 2026 - ISSN 2356-8569
http://dx.doi.org/10.21622/RESD.2026.12.1.1765

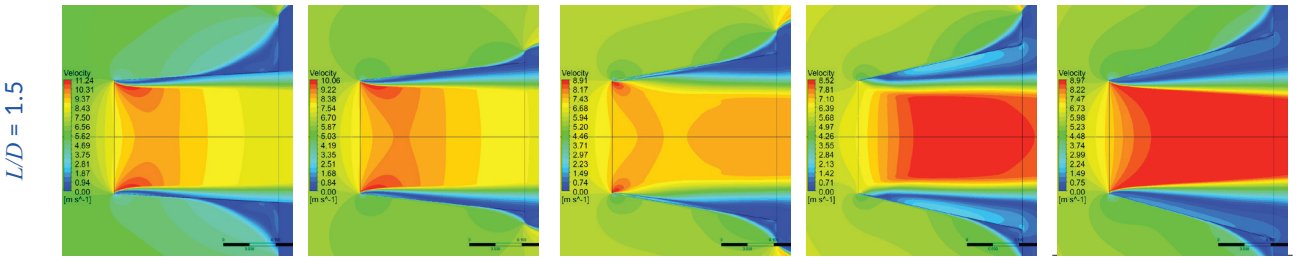

Figure 5: Velocity contours of twenty-five diverging diffuser models.

Table 3: Performance results of the Orthogonal array diffuser models

Model	L/D	α	h/D	V_R	m_n
C01	0.5	3	0.1	1.6	0.22
C02	0.5	6	0.2	1.48	0.27
C03	0.5	9	0.3	1.41	0.32
C04	0.5	12	0.4	1.39	0.38
C05	0.5	15	0.5	1.42	0.45
C06	0.75	3	0.2	1.68	0.35
C07	0.75	6	0.3	1.55	0.41
C08	0.75	9	0.4	1.48	0.48
C09	0.75	12	0.5	1.47	0.57
C10	0.75	15	0.1	1.35	0.36
C11	1	3	0.3	1.73	0.49
C12	1	6	0.4	1.62	0.58
C13	1	9	0.5	1.56	0.67
C14	1	12	0.1	1.42	0.46
C15	1	15	0.2	1.39	0.55
C16	1.25	3	0.4	1.8	0.64
C17	1.25	6	0.5	1.7	0.74
C18	1.25	9	0.1	1.55	0.57
C19	1.25	12	0.2	1.49	0.65
C20	1.25	15	0.3	1.43	0.76
C21	1.5	3	0.5	1.87	0.79
C22	1.5	6	0.1	1.68	0.64
C23	1.5	9	0.2	1.49	0.74
C24	1.5	12	0.3	1.42	0.87
C25	1.5	15	0.4	1.5	1

In equation 3, V = wind velocity, P_0 = stagnation pressure, P_s = static pressure, and ρ is the air density. Equation 3 is derived from Bernoulli's principle and is used when the pitot tube is used for the measurement of pressure drop. For the experimentation, the same input velocity of 6 m/s ($\Delta P_{initial}$ = 22 Pa) is taken as that taken for the CFD simulation. The pressure values are recorded at nine points at a radial plane placed at $0.2L$ from the diffuser inlet and presented in Table 4. Velocity values obtained using the recorded pressure values are also added to the table. This table also gives the CFD values and the percentage difference in experimental and CFD results. The experimental values vary from CFD, ranging from 3.82 to 6.07 % which can be considered as an acceptable agreement [47]. Experimental and CFD results of one diffuser model are also validated with the literature. Due to practical constraints related to experimental setup, manufacturing, and experimentation, only one model is tested and validated. These tabulated variations are also plotted in Fig. 6.

Table 4: Comparison of experimental and CFD radial velocities for diffuser model C01

Pitot Tube position (m)	$\Delta P = P_t - P_s$ (Pa)	V_{exp} (m/s)	VR_{exp}	V_{CFD} (m/s)	VR_{CFD}	Difference (%)
0.0	33.5	7.396	1.233	7.74	1.290	4.421
0.012	34	7.451	1.242	7.75	1.291	3.829
0.023	34	7.451	1.242	7.78	1.296	4.214
0.035	34.5	7.505	1.251	7.83	1.306	4.209
0.047	35	7.559	1.260	7.92	1.321	4.610
0.058	36	7.667	1.278	8.06	1.344	4.929
0.070	37.75	7.851	1.308	8.28	1.381	5.222
0.082	41.25	8.207	1.368	8.65	1.441	5.073
0.093	46.5	8.713	1.452	9.28	1.546	6.074

Volume 12, Issue 1, June 2026 - ISSN 2356-8569
http://dx.doi.org/10.21622/RESD.2026.12.1.1765

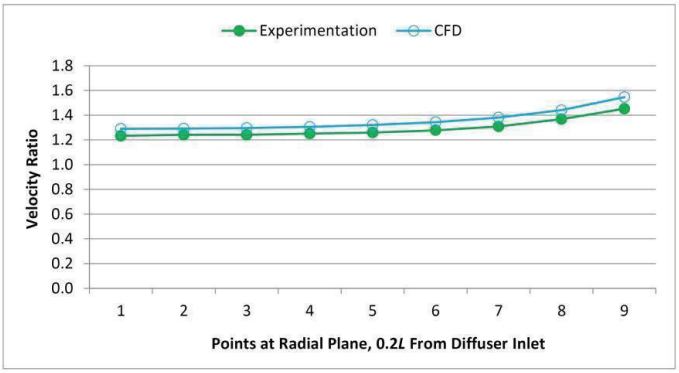

Figure 6: Velocity ratios obtained through CFD and wind tunnel experiments at a radial plane (0.2*L* from Diffuser Inlet).

IV. Discussion

The normal probability plot shows a good straight line agreement. The number of outliers in versus fit is not significantly different. It should be noted that the developed regression equation is valid only within the investigated ranges of design parameters and should not be used for extrapolation beyond these limits.

A. Effect of input variables on the velocity ratio

In the first to fifth columns of Fig. 5, values of α are increasing, and it is observed that for all lower values of α, higher velocities are obtained. Also, it is observed that velocity values are increasing with respect to L/D.

However, it is not sufficient to know about the influence of L/D, h/D, and α on the diffuser performance through visual observation and limited quantitative information from velocity contours. To get a detailed understanding, it is important to use suitable statistical techniques.

Hence, it is decided to use different techniques that will give a detailed evaluation of the results. Multivariate regression analysis and a Pareto chart are used to study the influencing factors and their intensity velocity ratio (V_R). The main effect plot is used to understand the effect of each factor on V_R. Further, to get optimum regions of better performance, 2D contours and surface plots are used.

Preliminary correlation checks are performed for these results before performing the multivariate regression analysis to get the mathematical relationship between input variables $(L/D,\ h/D,\ \alpha)$ and output variables $(V_R,\ m_n)$. The multivariate regression analysis will be useful to understand the effect of individual input variables and their interactive effect on the output variables.

For performing multivariate regression analysis, Minitab software is used. The data from Table 3 is used for this analysis. The relationship obtained for V_R is shown by Eq. (4). This equation consists of linear terms, nonlinear quadratic terms, and interaction terms. However, the interaction term $\alpha \times h/D$ is omitted because of its redundant nature. For other interactions, multi-collinearity is checked and found satisfactory. From the various coefficients obtained in the analysis, as shown in Table 5, it is seen that most of the linear as well as interaction terms have a P-value < 0.05, indicating their significant effect on velocity performance. The interaction term $L/D \times h/D$ has a P-value = 0.144 > 0.05, which indicates its non-significant effect on diffuser velocity performance.

Table 3: P-values for various terms in the regression equation for V_R

Term	L/D	α	h/D	$L/D \times L/D$	$\alpha \times \alpha$	$h/D \times h/D$	$L/D \times \alpha$	$L/D \times h/D$
P-Value	0.000	0.000	0.010	0.000	0.000	0.006	0.000	0.144

$$V_R = 1.5862 + 0.4558(L/D) - 0.05356(\alpha) - 0.3082(h/D) - 0.1409(L/D)^2 + 0.002246(\alpha)^2 + 0.625(h/D)^2 - 0.01303((L/D)\times\alpha) + 0.1528((L/D)\times(h/D)) \quad (4)$$

In this regression equation obtained for V_R, 1.5862 is the intercept. From the equation, it is observed that an increase in L/D significantly enhances the value of V_R. However, the negative quadratic term of L/D indicates that this velocity rise is up to a certain limit of L/D, and further increase in length does not contribute towards velocity improvement. This important result is also in line with the literature result [37]. The negative sign applied to the semi-expansion angle α in the equation indicates the reduction in V_R with increasing the amount of divergence. This result is well-matched with the fundamental concept of flow separation and energy loss because of the increasing expanding angle.

Volume 12, Issue 1, June 2026 - ISSN 2356-8569
http://dx.doi.org/10.21622/RESD.2026.12.1.1765

On the other hand, the quadratic term of α^2 has a positive sign with a coefficient of 0.002246, which indicates that an initial increment in α reduces the value of V_R; however, there can be an optimum value of expansion angle to enhance the diffuser performance. The flange height term h/D also shows a negative linear effect on the velocity ratio, just like α, but the effect is more dominant than that of α. In the combined effect, increasing values of L/D and α are causing opposite effects on the velocity rise, and as discussed earlier, the combined effect of $L/D \times h/D$ is not significant. R^2 and adjusted R^2 values are found as 99.84 % and 99.67 % respectively, which indicate the well-accepted accuracy of the regression model. The adjusted R^2 value is also very close to the R^2 value, which shows that the terms included in the model are justified and the regression model is robust and reliable. Further, the developed regression model is based on a structured experimental design with 25 systematically distributed cases having uniform parametric levels. The statistical significance of individual terms was checked using p-values, and non-significant terms are not considered in the final model. In the residual analysis, no abnormal trends or large deviations were observed, which shows the stability of the regression model.

To further understand the most influential parameters affecting the V_R, the Pareto chart showing the standardized effects from the analysis is presented in Fig. 7. In this chart, $A = L/D$, $B = \alpha$, $C = h/D$; AA, BB, CC are the quadratic terms; AB and AC are the interaction terms. From the chart, it is observed that the nonlinear term α^2 significantly changes the value of V_R among all other terms. Also, the linear *terms* α and L/D have strong effects. All terms AA, AB, and CC are more influential than the linear term h/D. The interaction term AC is also observed as non-significant, and its standardized effect is less than the significance threshold of 2.31.

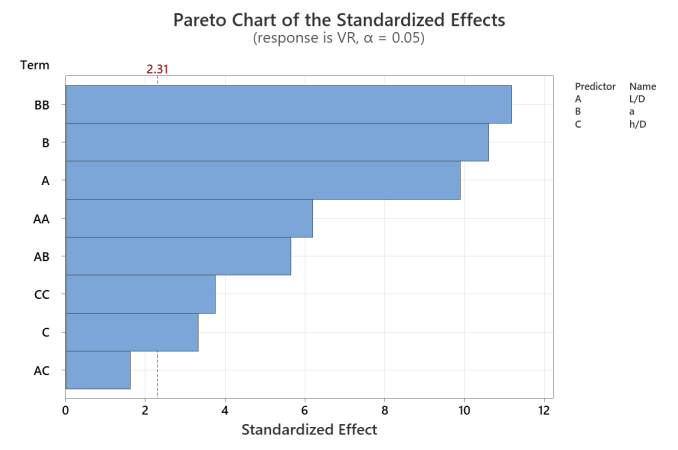

Figure 7: Pareto chart for standardized effect of various terms and interactions V_R ($A = L/D$, $B = \alpha$, $C = h/D$; AA, BB, CC - quadratic terms; AB and AC - interaction terms).

Here, it is also important to study how individual factors affect the V_R of these diffuser models. The main effect plot, as per Fig. 8, is a graphical representation of the effect of the individual input variables $(L/D, h/D, \alpha)$ on the velocity ratio. The mean V_R for each level of a factor is shown in this plot. A line joining the means of V_R for each level factor is useful to compare the influence at different levels.

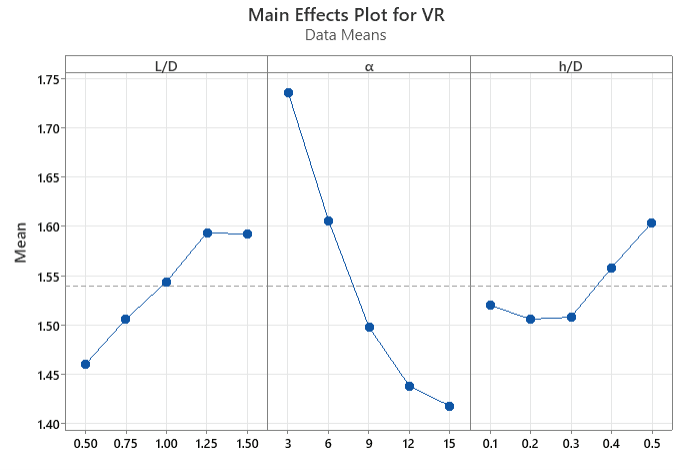

Figure 8: Main effect plot for V_R.

Volume 12, Issue 1, June 2026 - ISSN 2356-8569
http://dx.doi.org/10.21622/RESD.2026.12.1.1765

The main effect plot in Fig. 8 shows that when L/D increases from 0.5 to 1.25, V_R steadily increases and slightly stabilizes from 1.25 to 1.5. This statement matches well with the linear and quadratic terms results from the regression equation. Increasing the L/D beyond 1.25 does not contribute to enhancing V_R significantly. The second input variable α is the most sensitive variable and has a strong effect on the V_R. The V_R values drop suddenly as α changes from 3 ° to 15 °. The diffuser angle should be low and can be taken between 3 ° and 6 ° for better performance. The h/D values 0.2 and 0.3 are reducing the V_R, while 0.1 and 0.4 are delivering better performance compared to 0.2 and 0.3. Additionally, more flange height with an h/D ratio of 0.5 shows a slightly higher performance, which also increases the diffuser mass significantly and makes it inconvenient for practical application.

For further detailed evaluation of the interaction between two variables on the output, 3D surface response plots are used along with 2D contours, from which it is possible to identify the optimum zones, delivering better performance in terms of V_R. The effect of L/D and α on the velocity ratio V_R can be studied in detail from the 2D contour and 3D surface plot shown in Fig. 9 (a) and (b). The performance measured in terms of V_R is significantly influenced by the combination of L/D and α. For all levels of L/D, the highest values of V_R are observed at the semi-expansion angle α. In the low-angle region (3 ° to 6 °), values of V_R are considerably greater than those observed in angles more than 6 °. All red colored peaks show the values of maximum V_R at an angle of 3 ° and all five levels of the L/D.

For angles greater than 9 ° and lower L/D values, the effect of higher divergence is more adverse. Also, these plots show a clear nonlinear interaction between the L/D and α as per the regression models, and α is the most influential factor as observed in the Pareto chart. The 2D contour plot shows the left region, shown by green color shades, as an optimal design region for designing the diffuser with better performance. The region shown in black color shade cannot be preferred to get a better velocity rise. From the visual inspection of the plot, it is seen that at a lower α value around 3 ° and a diffuser L/D ratio of around 0.8 or more, the diffuser can deliver a better performance without increasing the mass considerably.

Figure 9 (c) and (d) show the 2D contours and 3D surface response plots for the relation between α and h/D to get the velocity enhancement in the form of V_R. From the 3D surface plots, it is observed that the peak V_R ratios (marked by red color) are obtained for all h/D ratios at α = 3 °. It also indicates that the α is an important parameter and shows an inverse effect in order to get better performance. From the 2D contour plot, it is clearly seen that the higher values of V_R are concentrated in the regions with low values of α (3 ° to 6 °) when the h/D values are between 0.1 and 0.15 approximately, and from 0.3 to 0.5. For h/D from 0.15 to 0.3, the lower values of V_R are observed.

Though the higher V_R values are observed for low α and higher h/D values, increased heights (h/D) make the diffuser bulky, costly, and inconvenient. Alternatively, it is beneficial to increase the diffuser length instead of flange height to get better performance if one wants to compromise for being overweight. The interaction between these two parameters indicates that a small diffuser angle and moderate flange height are able to deliver better performance. Hence, the observations obtained from these plots are in line with the regression equation and Pareto charts. Further, they provide more comprehensive observations as discussed here.

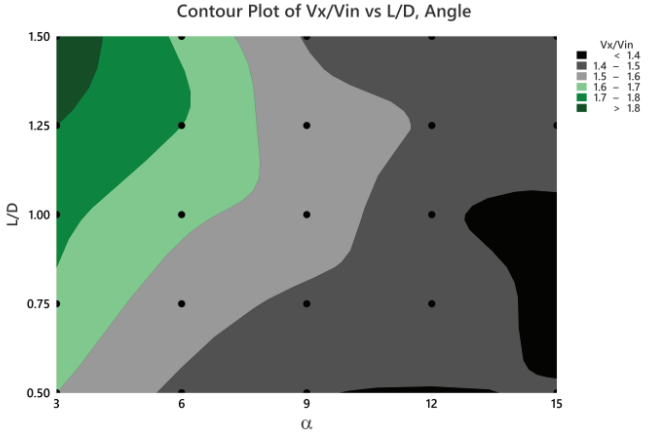

(a)

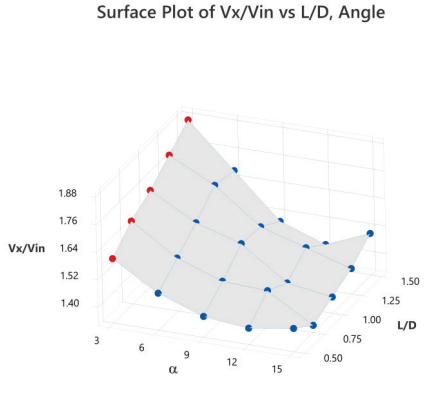

(b)

Volume 12, Issue 1, June 2026 - ISSN 2356-8569
http://dx.doi.org/10.21622/RESD.2026.12.1.1765

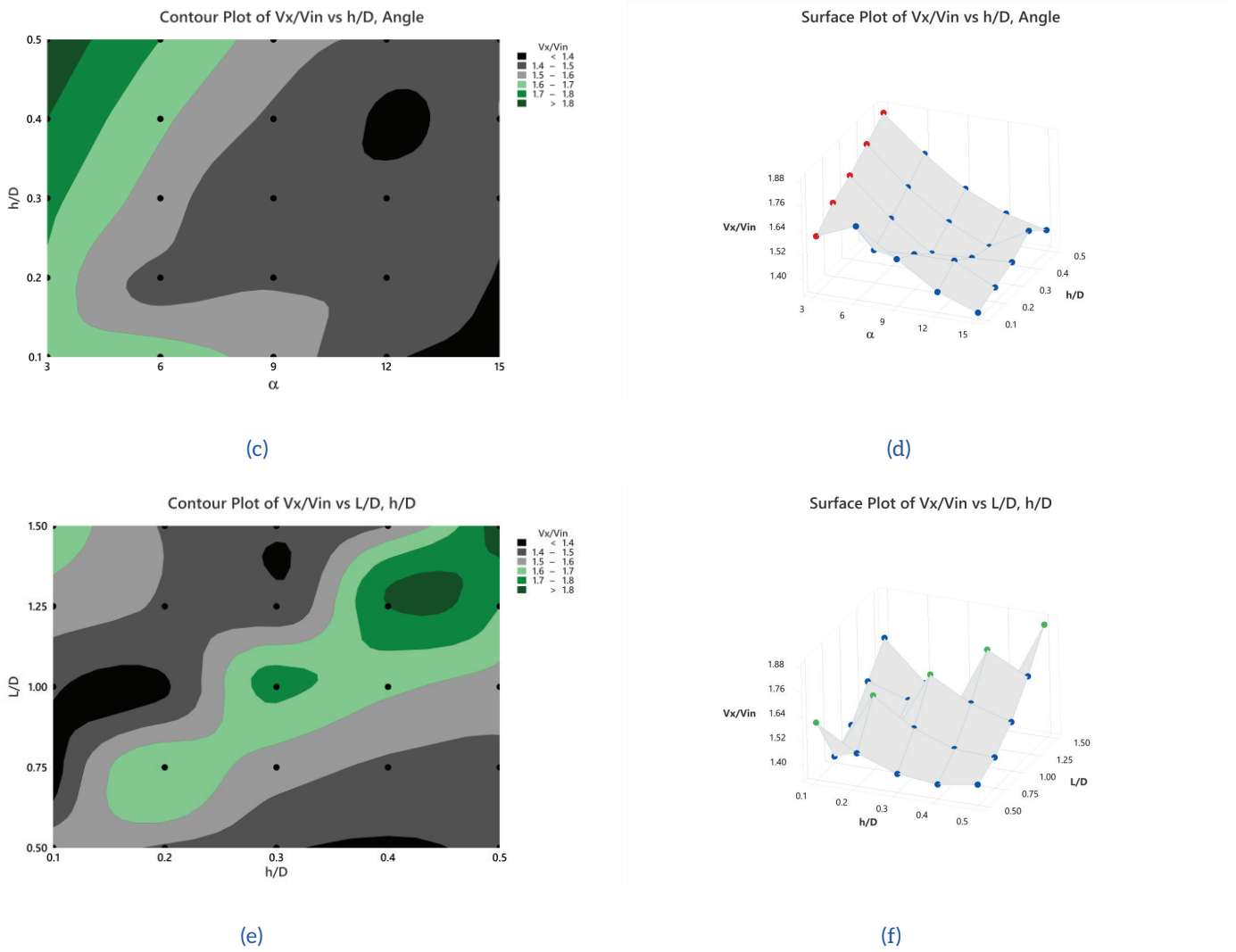

Figure 9: 2D contours and surface plots showing interactions among *L/D, h/D, α;* **a and b**) Contour and surface plot for *L/D and α;* c and d) Contour and surface plot for *h/D* and *α;* **e and f**) Contour and surface plot for *L/D* and *h/D.*

Fig. 9 (e) and (f) present the contour plot and response surface plot for the interaction of *L/D* and *h/D*. It is seen that higher V_R values lie along the diagonal region, as shown by green shades in the contour plot. It is also observed from the surface plot that these peak V_R values are indicated by green color points diagonally. Here, an important conclusion about *h/D* is observed from contour as well as surface plots. To get better V_R output, a diffuser with higher *L/D* values needs a higher *h/D*. This makes the diffuser bulky and overweight. Hence, an appropriate selection of the *L/D* ratio is required to make the diffuser compact with low weight. The mixed and random interaction is observed between these parameters, which is not too significant as obtained from *the P*-value.

B. Effect of input variables on normalized mass

In this research, the main objective is to enhance the value of V_R. On the other side, it is also important to minimize the diffuser mass. Here, diffuser masses are taken in non-dimensional form and termed as normalized mass (m_n). The brief discussion about m_n is presented in this section. From Table 3, it is observed that the m_n values are considerably changing, from 0.22 for the light diffuser to 1 for the heavy diffuser. Though it is obvious that the diffuser mass is increasing with all input dimensions, it is important to know about the effect of individual dimensions on the mass increment. From this study, it is possible to control the diffuser dimensions appropriately in order to maximize the V_R and minimize the m_n values.

Similar to V_R, the regression equation for m_n obtained from Minitab is shown by Eq. (5). From the *P*-values (0.23, 0.169, 0.281) it is seen that α^2, $(h/D)^2$ and $(L/D \times h/D)$ respectively are the non-significant

Volume 12, Issue 1, June 2026 - ISSN 2356-8569
http://dx.doi.org/10.21622/RESD.2026.12.1.1765

terms which is also observed from the regression equation and Pareto chart (Fig. 10). Further it is observed that the interaction term $(L/D \times \alpha)$ is the most influential term as increasing diffuser length with expanding angle increases circumferential mass of the diffuser. Further, the h/D is a linear term which is contributing to increasing diffuser mass significantly than individual L/D and α. The main significant effect of α^2, $(h/D)^2$, and $(L/D \times h/D)$ is not considerable.

$$m_n = 0.0907 + 0.1463(L/D) - 0.01741(\alpha) + 0.5696(h/D) + 0.0671(L/D)^2 + 0.000160(\alpha)^2 + 0.155(h/D)^2 + 0.02414((L/D)\times\alpha) + 0.0672((L/D)\times(h/D)) \quad (5)$$

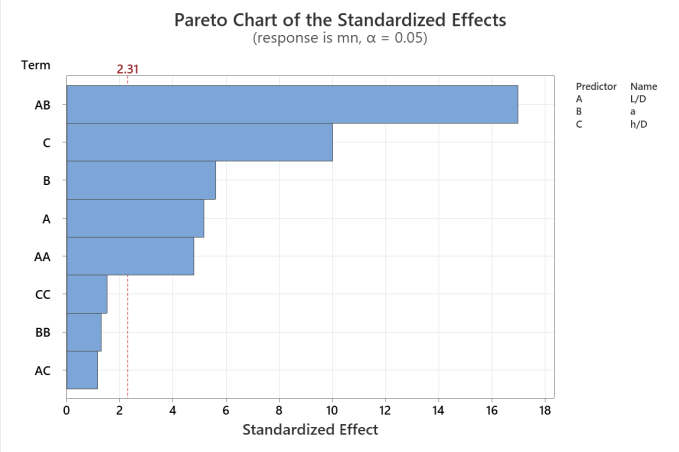

Figure 10: Pareto chart for standardized effect of various terms and interactions m_n ($A = L/D$, $B = \alpha$, $C = h/D$; AA, BB, CC - quadratic terms; AB and AC - interaction terms).

From the statistical techniques, it is observed that the linear term h/D alone does not significantly contribute to enhancing the V_R. On the other hand, it is one of the influencing linear terms in order to increase the diffuser mass. As discussed earlier, the increased diffuser mass makes the diffuser bulky, increases its cost, and also associated handling and installation difficulty.

The most important parameter affecting the mass of the diffuser is the combined parameter $L/D \times \alpha$. It can be seen that an increase in L/D ratio results in an increase in mass. However, an increase in the diffuser angle (α) enlarges the exit diameter, producing exactly the same effect. However, the requirements for enhancing the velocity ratio are contradictory requirements of these parameters. The results indicate that larger diffuser lengths and smaller diffuser angles are more favorable for velocity augmentation. Consequently, an optimal balance between these parameters must be achieved when selecting an appropriate diffuser configuration. The h/D ratio influences the flange height of the diffuser in a significant manner. An increase in flange height results in an improvement of the velocity ratio, based on findings of this work. However, the gain in velocity ratio is not very high. This means lower flange heights can be selected from a design perspective. Increasing the flange height causes the formation of low-pressure regions downstream of the diffuser, which contributes to flow acceleration.

C. Optimization of diffuser geometry using desirability function analysis

It is important to obtain the optimum dimensions of the diffuser $(L/D, h/D, \alpha)$, which can give a higher velocity ratio and lower diffuser mass. These two objectives (maximization of V_R and minimization of m_n) function problem is solved using the desirability function analysis (DFA) [54-56]. The optimization results obtained by desirability function analysis are shown in Fig. 11. For the optimized values $(L/D = 0.8636, h/D = 0.1$, and $\alpha = 3°)$, the composite desirability is obtained as 0.7100. The values of individual desirability for m_n and V_R are obtained as 0.83619 and 0.60280, respectively. This value of composite desirability indicates a reasonable balance between these two different objectives. A confirmation test is carried out to check the optimization results obtained from the desirability function analysis. Diffuser with these optimum dimensions is simulated using ANSYS, and the velocity contour plot for this new diffuser model is shown in Fig. 12. Values of V_R obtained from DFA and CFD are observed as 1.6793 and 1.6867, respectively. Only a 0.44 % variation was observed between these two values, which reports the accuracy of DFA.

When the performance of the optimized diffuser is compared with that of twenty-five diffuser models, it is observed that the optimized diffuser has better performance with low mass. For optimum diffuser normalized mass, m_n = 0.33, which is greater than only three diffusers' m_n values. Despite such low weight, its velocity ratio, V_R = 1.6867, is better than that of the twenty-one diffuser models. In many models, the velocity ratio is found to increase with

Volume 12, Issue 1, June 2026 - ISSN 2356-8569
http://dx.doi.org/10.21622/RESD.2026.12.1.1765

mass; however, the optimized model is showing a significantly compromised solution with low mass and better velocity performance, which also indicates the effectiveness of the optimization process.

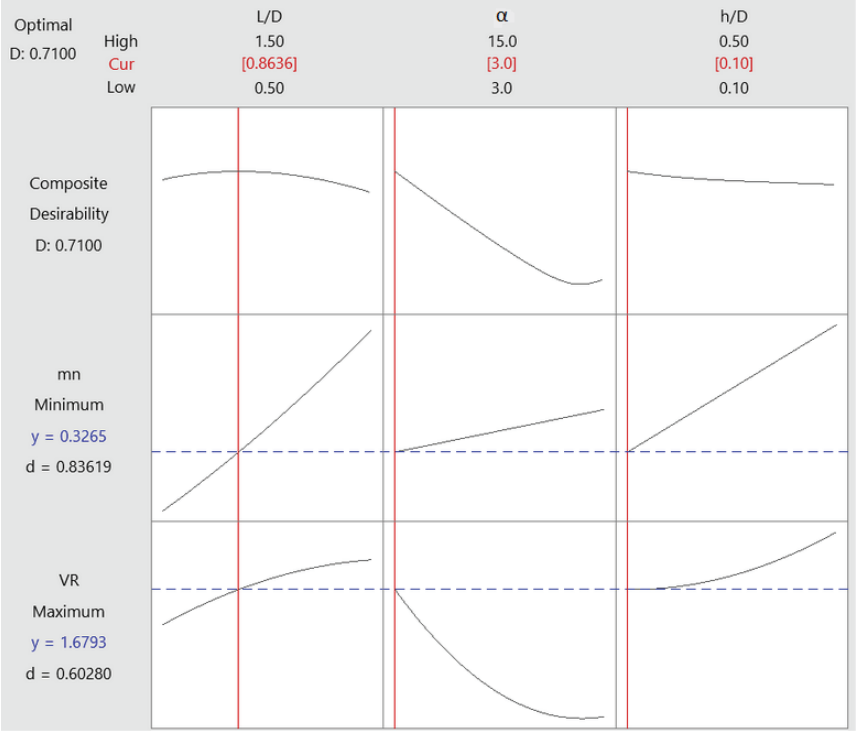

Figure 11: DFA plot for optimum diffuser dimensions.

For diffuser models C06, C11, C16, and C21, the V_R values are 1.68, 1.73, 1.80, and 1.87 with corresponding m_n values 0.35, 0.49, 0.64, and 0.79, respectively. Among these, diffuser model C06 has V_R and m_n values close to those of the optimum diffuser. However, the optimum diffuser has a flange height of 0.1 D while C06 has a flange height of 0.2 D. Although having more length of 0.8636D, the optimum diffuser still has a lower mass compared to C06. Though the velocity performance of C11, C16, and C21 is better than the optimized diffuser by 2.37, 6.51, and 10.65 % respectively, their normalized masses are 50.08, 96.02, and 141.96 % significantly higher. Therefore, a slight compromise in velocity performance is acceptable when it significantly reduces mass, avoiding the associated bulkiness, cost, and handling difficulties.

From this research work, the effect of three input variables, L/D, h/D, and α, each studied at five levels, on velocity performance and normalized mass is identified. Though the major weightage is given to velocity performance in order to get better performance, the effect on mass is also discussed. The long diffuser (with higher L/D up to a certain level) and low semi-expansion angles are linearly contributing to increase the velocity ratio, and h/D is contributing with mixed performance. However, it is important to decide the values of these variables considering their quadratic and interaction terms. A quadratic term of α is the major influencing factor for better velocity output. The quadratic term of L/D has a medium effect on the velocity performance. The interaction term of L/D and α is the most influential factor for mass. Also, flange height is a linearly influencing term for the mass at the second level.

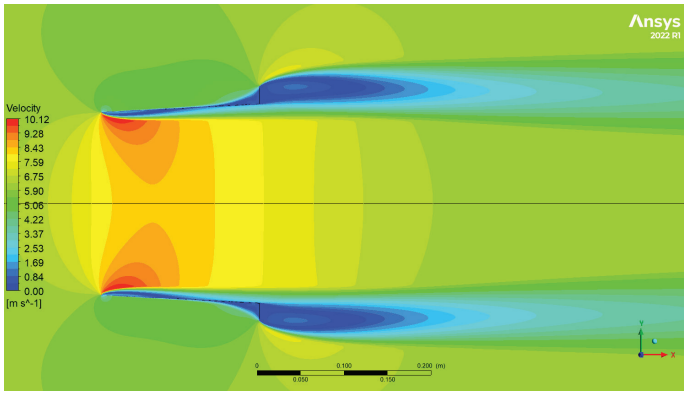

Figure 12: Velocity contour for optimized diffuser model.

Volume 12, Issue 1, June 2026 - ISSN 2356-8569
http://dx.doi.org/10.21622/RESD.2026.12.1.1765

Hence, a good consideration is required to select these values to get a higher velocity and lower mass. Lower mass not only results in the low cost, but it also increases durability, environmentally friendly positive impact, handling, and installation ease, and further increases acceptance for placing them in actual applications. From the DFA, it is also observed that the intermediate value of diffuser length and lower values of expansion angle and flange height deliver compromised performance in terms of velocity output and reduce the diffuser mass.

The velocity ratio is a major criterion in selecting the right diffuser geometry, as it largely affects flow uniformity and aerodynamic performance. However, in practical applications, things like handling, transportation, and installation of diffusers are also critical. Larger or bulky diffusers not only face challenges during installation but can also increase lift and/or drag forces depending on the design. Therefore, this adds to additional structural requirements and thus increases overall system cost. Hence, the diffuser's velocity ratio is therefore assigned greater relative importance as performance is considered. The next significant factor is the diffuser mass that must be considered in the optimization. This shows the need to ensure ease of handling and broader practical applicability. A balanced consideration of these objectives helps design that are not only aerodynamically efficient but also feasible for large-scale applications. In large-scale applications, ease of handling and better cost-effectiveness significantly influence diffuser adoption.

V. Conclusion

In this research, a total of 25 flanged diverging diffuser models for small wind turbines were analyzed using CFD to study the effect of three-dimensional parameters L/D, h/D, and α on the velocity enhancement and diffuser mass. CFD results were validated from the experimental results of a diffuser model, C01, and have shown a good, acceptable agreement from 3.8 to 6.0 %.

Further analysis of CFD results of 25 models using statistical techniques, including multivariate regression equation, Pareto chart, main effect plot, 2D contours, and 3D response surface graphs. Among the three input variables, semi-expansion angle, α, is established as the most important parameter (its linear as well as quadratic term), whose lower values contribute to getting a better velocity ratio V_R. The higher L/D value increases the velocity ratio up to a certain level and then shows no significant effect.

An important conclusion about a flange height is also drawn from the surface response plot. For increased diffuser length, greater flange height is required in order to get better performance. On the other hand, it also indicates that in such cases, the diffuser becomes bulky and costly. The cumulative effect of diffuser length and semi-expansion angle has a substantial effect on increasing the diffuser mass, and increasing flange height also increases the diffuser mass considerably.

It is important to select appropriate dimensions of a diverging diffuser to get a better compromise result for increased velocity and reduced diffuser mass, as shown by desirability function analysis. This analysis suggests the selection of mid-level length and low values of semi-expansion angle and flange height with better-compromised performance. Compared to slightly higher performing models C11, C16, and C21, the optimized diffuser shows substantial mass reduction with low bulkiness and cost. Such a lightweight and compact diffuser design is particularly suitable for practical application, where ease of installation and material cost are important considerations.

Conflict of interest

The authors declare that they have no known competing financial interests or personal relationships that could have appeared to influence the work reported in this paper.

References

[1] A. Khedr, "Bio-mimicry in the aerodynamics of small horizontal axis wind turbines," *Sustainable Energy Technologies and Assessments*, vol. 76, p. 104260, Apr. 2025, doi: 10.1016/j.seta.2025.104260.

[2] R. S. Hiware and P. M. Daigavane, "Super capacitor-enhanced neural control (SENCO) for power quality optimization in wind turbine-integrated microgrids," *Renewable Energy and Sustainable Development*, vol. 11, no. 2, p. 273, Aug. 2025, doi: 10.21622/resd.2025.11.2.1279.

[3] A. E. Faisal *et al.*, "Investigating the techniques used for improving the aerodynamic performance of Archimedes spiral wind turbines: A comprehensive review and future work avenues," *Results in Engineering*, vol. 25, p. 103992, Mar. 2025, doi: 10.1016/j.rineng.2025.103992.

[4] M. A. Kadhim *et al.*, "Performance study of low-speed wind energy harvesting by micro wind turbine system," *Energy Reports*, vol. 13, pp. 3712–3727, Jun. 2025, doi: 10.1016/j.egyr.2025.02.046.

[5] P. S. Kumar, C. Chandrika, P. K. Rao, P. K. Rao, and S. K. Oruganti, "Interpretable hybrid machine learning models for renewable-powered smart grid stability prediction," *Renewable Energy and Sustainable Development*, vol. 11, no. 2, p. 397, Oct. 2025, doi: 10.21622/resd.2025.11.2.1509.

[6] A. F. Alajmi and M. Ramulu, "The effectiveness of graphene and polyurethane multilayer coating on minimizing the leading-edge erosion of wind turbine blades," *Results in Engineering*, vol. 26, p. 104804, Jun. 2025, doi: 10.1016/j.rineng.2025.104804.

[7] T. D. Oliveira, L. A. Tofaneli, and A. Á. B. Santos, "Aerodynamic optimization of small diffuser Augmented Wind Turbines: A differential evolution approach," *Energy Conversion and Management: X*, vol. 26, p. 100891, Apr. 2025, doi: 10.1016/j.ecmx.2025.100891.

[8] M. Saleem, M. T. Bin-Saleem, M. A. Bin-Saleem, M. Ali, and E. N. Mahrous, "Energy transition in Saudi Arabia: harnessing solar solutions for a sustainable future renewable energy blend while navigating challenges and capitalizing on opportunities," *Renewable Energy and Sustainable Development*, vol. 11, no. 2, p. 190, Aug. 2025, doi: 10.21622/resd.2025.11.2.1319.

[9] O. M. Abo Gabl, M. Y. Morgan, and M. S. El-Sobki (Jr.), "Decentralized economic operation of isolated AC, DC, and hybrid microgrids," *Renewable Energy and Sustainable Development*, vol. 11, no. 2, p. 175, Aug. 2025, doi: 10.21622/resd.2025.11.2.1289.

[10] H. Hamid and R. M. Abd El Maksoud, "A numerical assessment of the heterogeneous effects of innovative shroud profiles for horizontal axis wind turbine," *Heliyon*, vol. 11, no. 2, p. e41661, Jan. 2025, doi: 10.1016/j.heliyon.2025.e41661.

[11] F. Avallone, D. Ragni, and D. Casalino, "On the effect of the tip-clearance ratio on the aeroacoustics of a diffuser-augmented wind turbine," *Renew. Energy*, vol. 152, pp. 1317–1327, Jun. 2020, doi: 10.1016/j.renene.2020.01.064.

[12] M. S. Sadeq and M. S. Kassim, "Experimental investigation of axial-flow turbine performance using water and oil: effects of rotation speed, blade count, and oil pre-heating," *Renewable Energy and Sustainable Development*, vol. 11, no. 2, p. 301, Sep. 2025, doi: 10.21622/resd.2025.11.2.1445.

[13] S. A. Abdollahi, S. F. Ranjbar, M. Jafarai, M. B. Ehghaghi, and S. Faramarzi, "Enhancing wind energy efficiency: A study on the power output of shrouded wind turbines for a hydrogen storage system," *Results in Engineering*, vol. 26, p. 104710, Jun. 2025, doi: 10.1016/j.rineng.2025.104710.

[14] Z. A. Shawket and S. H. Danook, "Overview improving the efficiency of a wind turbine by using a nozzle and solar radiation," *Unconventional Resources*, vol. 7, p. 100191, Jul. 2025, doi: 10.1016/j.uncres.2025.100191.

[15] Riyanto *et al.*, "The Performance of Shrouded Wind Turbine at Low Wind Speed Condition," *Energy Procedia*, vol. 158, pp. 260–265, Feb. 2019, doi: 10.1016/j.egypro.2019.01.086.

[16] B. Y. Kassa, A. T. Baheta, and A. Beyene, "Current Trends and Innovations in Enhancing the Aerodynamic Performance of Small-Scale, Horizontal Axis Wind Turbines: A Review," *ASME Open Journal of Engineering*, vol. 3, Jan. 2024, doi: 10.1115/1.4064141.

[17] H. M. Elbakry, A. A. A. Attia, O. E. Abdellatif, and M. S. Zahran, "Simulation of Shrouded Wind Turbine Performance," in *World Congress on Sustainable Technologies (WCST-2024)*, Infonomics Society, Dec. 2024, pp. 162–169. doi: 10.20533/WCST.2024.0011.

[18] M. R. Mahajan and S. D. Nikhade, "COMPUTATIONAL AND EXPERIMENTAL RESEARCH ON CONICAL DIVERGING DIFFUSERS FOR ENHANCING WIND TURBINE PERFORMANCE: A COMPREHENSIVE REVIEW," *Proceedings on Engineering Sciences*, vol. 7, no. 3, pp. 2113–2126, Sep. 2025, doi: 10.24874/PES07.03B.012.

[19] Agha A., Chaudhry H. N., and Wang F., "Diffuser Augmented Wind Turbine (DAWT) Technologies: A Review," *International Journal of Renewable Energy Research*, no. v8i3, 2018, doi: 10.20508/ijrer.v8i3.7794.g7436.

[20] J. Taghinezhad, S. Abdoli, V. Silva, S. Sheidaei, R. Alimardani, and E. Mahmoodi, "Computational fluid dynamic and response surface methodology coupling: A new method for optimization of the duct to be used in ducted wind turbines," *Heliyon*, vol. 9, no. 6, p. e17057, Jun. 2023, doi: 10.1016/j.heliyon.2023.e17057.

[21] S. Sridhar, M. Zuber, S. S. B., A. Kumar, E. Y. K. Ng, and J. Radhakrishnan, "Aerodynamic comparison of slotted and non-slotted diffuser casings for Diffuser Augmented Wind Turbines (DAWT)," *Renewable and Sustainable Energy Reviews*, vol. 161, p. 112316, Jun. 2022, doi: 10.1016/j.rser.2022.112316.

[22] M. M. Naji and B. A. Jabbar, "Diffuser augmented wind turbine: A review study," in *AIP Conference Proceedings*, 2024, p. 100015. doi: 10.1063/5.0191895.

[23] D. A. Teklemariyem, E. T. Yimer, V. R. Ancha, and B. A. Zeru, "Parametric study of an empty diffuser geometric parameters and shape for a wind turbine using CFD analysis," *Heliyon*, vol. 10, no. 5, p. e26782, Mar. 2024, doi: 10.1016/j.heliyon.2024.e26782.

[24] S. E. Hosseini and Z. Saboohi, "Ducted wind turbines: A review and assessment of different design models," *Wind Engineering*, vol. 49, no. 3, pp. 833–854, Jun. 2025, doi: 10.1177/0309524X241282090.

[25] D. Li, C. Li, W. Zhang, and H. Zhu, "Effect of building diffusers on aerodynamic performance for building augmented vertical axis wind turbine," *Journal of Renewable and Sustainable Energy*, vol. 13, no. 2, Mar. 2021, doi: 10.1063/5.0025742.

[26] S. Ahmad, W. Rafat Al, A. M El Haj, K. Khalil, and S. Muath NA Bani, "Analysis of Accelerating Devices for Enclosure Wind Turbines," *International Journal of Astronautics and Aeronautical Engineering*, vol. 2, no. 2, Dec. 2017, doi: 10.35840/2631-5009/7509.

[27] M. T. S. Badawy and M. E. Aly, "Gas dynamic analysis of the performance of diffuser augmented wind turbine," *Sadhana*, vol. 25, no. 5, pp. 453–461, Oct. 2000, doi: 10.1007/BF02703626.

[28] K. Abe and Y. Ohya, "An investigation of flow fields around flanged diffusers using CFD," *Journal of Wind Engineering and Industrial Aerodynamics*, vol. 92, no. 3–4, pp. 315–330, Mar. 2004, doi: 10.1016/j.jweia.2003.12.003.

[29] T. Matsushima, S. Takagi, and S. Muroyama, "Characteristics of a highly efficient propeller type small wind turbine with a diffuser," *Renew. Energy*, vol. 31, no. 9, pp. 1343–1354, Jul. 2006, doi: 10.1016/j.renene.2005.07.008.

[30] Y. Ohya, T. Karasudani, A. Sakurai, K. Abe, and M. Inoue, "Development of a shrouded wind turbine with a flanged diffuser," *Journal of Wind Engineering and Industrial Aerodynamics*, vol. 96, no. 5, pp. 524–539, May 2008, doi: 10.1016/j.jweia.2008.01.006.

[31] B. Kosasih and A. Tondelli, "Experimental Study of Shrouded Micro-Wind Turbine," *Procedia Eng.*, vol. 49, pp. 92–98, 2012, doi: 10.1016/j.proeng.2012.10.116.

[32] D. L. M. Barbosa *et al.*, "A PROPOSED MATHEMATICAL MODEL FOR THE VELOCITY PROFILE INTERNALLY TO A CONICAL DIFFUSER," *Revista de Engenharia Térmica*, vol. 12, no. 2, p. 69, Dec. 2013, doi: 10.5380/reterm.v12i2.62050.

[33] S. A. H. Jafari and B. Kosasih, "Flow analysis of shrouded small wind turbine with a simple frustum diffuser with computational fluid dynamics simulations," *Journal of Wind Engineering and Industrial Aerodynamics*, vol. 125, pp. 102–110, Feb. 2014, doi: 10.1016/j.jweia.2013.12.001.

[34] S. Z. Roshan, S. Alimirzazadeh, and M. Rad, "RANS simulations of the stepped duct effect on the performance of ducted wind turbine," *Journal of Wind Engineering and Industrial Aerodynamics*, vol. 145, pp. 270–279, Oct. 2015, doi: 10.1016/j.jweia.2015.07.010.

[35] M. Lipian, M. Karczewski, and K. Olasek, "Sensitivity study of diffuser angle and brim height parameters for the design of 3 kW Diffuser Augmented Wind Turbine," *Open Engineering*, vol. 5, no. 1, Aug. 2015, doi: 10.1515/eng-2015-0034.

[36] K. Olasek, M. Karczewski, M. Lipian, P. Wiklak, and K. Józwik, "Wind tunnel experimental investigations of a diffuser augmented wind turbine model," *Int. J. Numer. Methods Heat Fluid Flow*, vol. 26, no. 7, pp. 2033–2047, Sep. 2016, doi: 10.1108/HFF-06-2015-0246.

[37] P.-M. Masukume, G. Makaka, and D. Tinarwo, "To cite this article: Peace-Maker Masukume, Golden Makaka, David Tinarwo. Optimum Geometrical Shape Parameters for Conical Diffusers in Ducted Wind Turbines," *International Journal of Energy and Power Engineering*, vol. 5, no. 6, 2016.

[38] I. F. Zidane, K. M. Saqr, G. Swadener, X. Ma, and M. F. Shehadeh, "On the role of surface roughness in the aerodynamic performance and energy conversion of horizontal wind turbine blades: a review," *Int. J. Energy Res.*, vol. 40, no. 15, pp. 2054–2077, Dec. 2016, doi: 10.1002/er.3580.

[39] A. M. El-Zahaby, A. E. Kabeel, S. S. Elsayed, and M. F. Obiaa, "CFD analysis of flow fields for shrouded wind turbine's diffuser model with different flange angles," *Alexandria Engineering Journal*, vol. 56, no. 1, pp. 171–179, Mar. 2017, doi: 10.1016/j.aej.2016.08.036.

[40] Zidane I. F., Swadener G., Saqr K. M., Ma X., and Shehadeh M. F., "CFD investigation of transitional separation bubble characteristics on NACA 63415 airfoil at low Reynolds numbers," in *Proc. 25th UKACM Conf. on Computational Mechanics*, Birmingham, U.K, 2017.

[41] I. F. Zidane, K. M. Saqr, G. Swadener, X. Ma, and M. F. Shehadeh, "Computational fluid dynamics study of dusty air flow over NACA 63415 airfoil for wind turbine applications," *J. Teknol.*, vol. 79, no. 7–3, 2017, doi: 10.11113/jt.v79.11877.

[42] P.-M. Masukume, G. Makaka, and P. Mukumba, "Optimization of the Power Output of a Bare Wind Turbine by the Use of a Plain Conical Diffuser," *Sustainability*, vol. 10, no. 8, p. 2647, Jul. 2018, doi: 10.3390/su10082647.

[43] M. Takey, T. Mat Lazim, I. S. Ishak, N. A. R. Nik Mohd, and N. Othman, "Computational Investigation of a Wind Turbine Shrouded with a Circular Ring," *CFD Letters*, vol. 12, no. 10, pp. 40–51, Nov. 2020, doi: 10.37934/cfdl.12.10.4051.

[44] I. F. Zidane, G. Swadener, X. Ma, M. F. Shehadeh, M. H. Salem, and K. M. Saqr, "Performance of a wind turbine blade in sandstorms using a CFD-BEM based neural network," *Journal of Renewable and Sustainable Energy*, vol. 12, no. 5, Sep. 2020, doi: 10.1063/5.0012272.

[45] A. İlhan, H. Zontul, S. Tümse, M. Bilgili, and B. Şahin, "Flow analyses of diffuser augmented wind turbines," *Energy Sources, Part A: Recovery, Utilization, and Environmental Effects*, vol. 46, no. 1, pp. 1102–1126, Dec. 2024, doi: 10.1080/15567036.2020.1861130.

[46] J. N. Mohanan, K. Sundaramoorthy, and A. Sankaran, "Performance Improvement of a Low-Power Wind Turbine Using Conical Sections," *Energies (Basel).*, vol. 14, no. 17, p. 5233, Aug. 2021, doi: 10.3390/en14175233.

[47] M. A. Rahmatian, P. Hashemi Tari, M. Mojaddam, and S. Majidi, "Numerical and experimental study of the ducted diffuser effect on improving the aerodynamic performance of a micro horizontal axis wind turbine," *Energy*, vol. 245, p. 123267, Apr. 2022, doi: 10.1016/j.energy.2022.123267.

[48] I. F. Zidane, H. M. Ali, G. Swadener, Y. A. Eldrainy, and A. I. Shehata, "Effect of upstream deflector utilization on H-Darrieus wind turbine performance: An optimization study," *Alexandria Engineering Journal*, vol. 63, pp. 175–189, Jan. 2023, doi: 10.1016/j.aej.2022.07.052.

[49] A. Abdallah, M. A. William, and I. F. Zidane, "Elevating Wind Energy Harvesting with J-shaped Blades: A CFD- driven Analysis of H-Darrieus Vertical Axis Wind Turbines," *International Maritime Transport and Logistic Journal*, vol. 13, no. 0, p. 233, Aug. 2024, doi: 10.21622/MARLOG.2024.13.1.108.

[50] A. Abdallah, M. A. William, N. A. Moharram, and I. F. Zidane, "Boosting H-Darrieus vertical axis wind turbine performance: A CFD investigation of J-Blade aerodynamics," *Results in Engineering*, vol. 27, 2025, doi: 10.1016/j.rineng.2025.106358.

[51] S. Sanaye and A. Farvizi, "Optimizing a vertical axis wind turbine with helical blades: Application of 3D CFD and Taguchi method," *Energy Reports*, vol. 12, pp. 2527–2547, Dec. 2024, doi: 10.1016/j.egyr.2024.08.059.

[52] L. Benahmed, K. Aliane, B. Rostane, and S. Abboudi, "Numerical analysis of baffles on geothermal energy in a U-shaped heat exchanger," *Renewable Energy and Sustainable Development*, vol. 11, no. 1, p. 27, Jan. 2025, doi: 10.21622/resd.2025.11.1.1150.

[53] M. R. Mahajan, S. D. Nikhade, and S. A. Kale, "Comparative Assessment of Selected Straight Conical Diffuser Models for Small Wind Turbine," *Journal of Engineering Science and Technology Review*, vol. 18, no. 6, pp. 22–31, 2025, doi: 10.25103/jestr.186.03.

[54] M. M. Awd Allah and M. A. Abd El-baky, "Multi-objective optimization through desirability function analysis on the crashworthiness performance of thermoplastic/thermoset hybrid structures," *Compos. B Eng.*, vol. 284, p. 111742, Sep. 2024, doi: 10.1016/j.compositesb.2024.111742.

[55] K. Elsayed and C. Lacor, "CFD modeling and multi-objective optimization of cyclone geometry using desirability function, artificial neural networks and genetic algorithms," *Appl. Math. Model.*, vol. 37, no. 8, pp. 5680–5704, Apr. 2013, doi: 10.1016/j.apm.2012.11.010.

[56] M. Kariminejad, D. Tormey, C. Ryan, C. O'Hara, A. Weinert, and M. McAfee, "Single and multi-objective real-time optimisation of an industrial injection moulding process via a Bayesian adaptive design of experiment approach," *Sci. Rep.*, vol. 14, no. 1, p. 29799, Nov. 2024, doi: 10.1038/s41598-024-80405-2.